Performance improvement of small Unmanned Aerial Vehicles through gust energy harvesting

Nikola Gavrilovic, Emmanuel Bénard, Philippe Pastor, Jean-Marc Moschetta

Performance Improvement of Small Unmanned Aerial Vehicles Through Gust Energy Harvesting

Nikola Gavrilovic,* Emmanuel Benard,† Philippe Pastor,† and Jean-Marc Moschetta‡
Institut Supérieur de l'Aéronautique et de l'Espace–SUPAERO, 31055 Toulouse, France

DOI: 10.2514/1.C034531

Fixed-wing miniature aerial vehicles usually fly at low altitudes that are often exposed to turbulent environments. Gust soaring is a flight technique of energy harvesting in such a complex and stochastic domain. The presented work shows the feasibility and benefits of exploiting a nonstationary environment for a small unmanned aerial vehicle. A longitudinal dynamics trajectory is derived, showing significant benefits in extended flight with a sinusoidal wind profile. An optimization strategy for active control is performed, with the aim of obtaining the most effective set of gains for energy retrieval. Moreover, a three-dimensional multipoint model confirms the feasibility of energy harvesting in a more complex spatial wind field. The influence of unsteady aerodynamics is determined on the overall energy gain along the flight path with active proportional control. The aerodynamic derivatives describing the contribution to lift by a change in angle of attack and elevator deflection are identified as the most contributing aerodynamic parameters for energy harvesting in a gusty environment, and are therefore suggested as a basic objective function of an unmanned aerial vehicle design for such a flight strategy.

Nomenclature

A, B	=	adjustable constants
b	=	section half-cord, m
C	=	coherence function
C_D	=	drag coefficient
C_L	=	lift coefficient
C_T	=	thrust coefficient
$C_1, C_2, \ldots, C_6$	=	polar coefficients
D	=	drag force, N
D_r	=	ratio of separation
E	=	specific energy, J/kg
E_t	=	endurance, s
F_α	=	low-frequency spectrum
J	=	transfer function
k	=	reduced frequency
k_w	=	wave number
k_g	=	sinusoidal gust amplitude, m/s
$k_1, k_2, \ldots, k_n$	=	control gains
L	=	lift force, N
L_c	=	coherence scale parameter
M	=	moment, N · m
m	=	mass, kg
n	=	load factor
P	=	specific power, $J/(kg^{-1} \cdot s^{-1})$
q	=	dynamic pressure, Pa
T	=	thrust force, N
t	=	time, s
U_o	=	average wind speed, m/s
V	=	airspeed, m/s
W	=	weight, N
w_x, w_z, w_y	=	longitudinal, vertical, and lateral components, m/s
X	=	vehicle horizontal position, m
Y	=	vehicle lateral position, m
Z	=	vehicle vertical position, m
ω_g	=	sinusoidal gust frequency
α	=	angle of attack, deg
γ	=	flight-path angle, deg
δ	=	control activation angle, deg
θ	=	pitch angle, deg
σ	=	intensity of fluctuations
ϕ	=	roll angle, deg
ψ	=	yaw angle, deg

Subscripts

a	=	air-mass referenced
e	=	elevator
f	=	flaps
i	=	vector/component expressed in inertial frame
m	=	spectral peak
nc	=	noncirculatory

I. Introduction

RECENT works driven by the unfailing experience from nature have shown a significant amount of energy available in the atmosphere. This energy is coming through in the form of vertical air motions described as spatial gradients, such as thermals, shear layers, orographic lift, and short-period temporal gradients as (for example) gusts. There are strong indications that birds use their feathers for sensing flow perturbations over their wingspan [1]. Being fluffy and subjected to fluttering provoked by small disturbances, birds have a natural sensory system according to Videler [2], which enables them to feel flow disorders along the wing, even before an inertial response. Eventual immediate action due to surface pressure fluctuations by modifying the wing geometry or profile curvature allows a quick and effective response in a gusty environment. However, for a variety of reasons, it is understood that identical copies from nature to manmade technologies are not feasible. Instead, a creative inspiration and conversion into technology are often based on various steps of abstraction.

One of the key objectives in the process of unmanned aerial vehicle (UAV) design is long-endurance flight. The flight technique inspired from albatrosses in the form of an optimal trajectory in the presence of wind gradients promises neutral energy cycles. On the other hand, gust soaring promises a quiet attractive flight strategy for endurance

*Doctoral Candidate, Department of Aerodynamics, Energetics and Propulsion, 10 Avenue Edouard-Belin BP 54032, CEDEX 4. Student Member AIAA.

†Associate Professor, Department of Aerospace Vehicles Design and Control, 10 Avenue Edouard-Belin BP 54032, CEDEX 4.

‡Full Professor, Department of Aerodynamics, Energetics and Propulsion, 10 Avenue Edouard-Belin BP 54032, CEDEX 4.

enhancement because it does not require any path planning or veer off the course. The performance of small UAVs being constrained by onboard energy due to their limited size can be significantly enhanced by specific flight strategies according to expected atmospheric formations or even continuous disturbances. UAVs have already proven the useful side of their exploitation, and our goal here is to extend their operability without disturbing the defined mission objectives in any flight case scenario. Most of the energy harvesting methods rely on an active control system that detects and exploits the energy of atmospheric turbulence through intentional maneuvering of the aircraft. It was demonstrated that exploitation of the energy available in the atmosphere requires responses that are usually beyond human capabilities, implying an autopilot with active control. Despite the fact that conventional approach was based on the mitigation of gust effects, such an exploitation presents a considerable opportunity to improve the already degraded performance of small UAVs.

This paper aims at providing a clear picture of the physics involved in the energy extraction mechanisms in the case of gust soaring, implementing three-dimensional and unsteady effects. It takes advantage of modern-day powerful computational resources, approaching a more realistic flight case scenario and evaluation of possible benefits. The following sections of the paper are organized as follows. Section II covers recent developments in the field of soaring strategies related to gusts. Section III briefly describes the artificial generation of a gust environment, pointing out the benefits of empirical methods. Section IV reveals a system of differential equations of motion, an active control strategy, and a dynamic energy transfer between aircraft and the atmosphere for unsteady aerodynamics. Section V quantifies the benefits of gust soaring, showing the aerodynamic parameters of the aircraft that affect energy gain. Finally, conclusions are presented in Sec. VI.

II. Related Research

A significant amount of work has been already reported for static soaring. One of the most famous strategies is certainly known as the MacCready [3] speed to fly theory. It was recently shown by Makovin and Langelaan [4] that the optimal cruising speed for maximizing the endurance of loitering flight in the presence of a quasi-stationary wind (thermals) varies between the best L/D ratio and the MacCready speed, depending on the thermal strength of a given cycle and the time required to fly some distance to a thermal and climb back up to the starting altitude. Previous work performed by Patel and Kroo [5] examined the way of energy harvesting from vertical turbulence by the active control of flaperons. Work from Langelaan [6,7] and Depenbusch and Langelaan [8] used a longitudinal vehicle model with optimized control in both sinusoidal and Dryden turbulence profiles. The development of an energy equation by Langelaan [6] and Lawrence and Sukkarieh [9] showed that certain maneuvers were necessary in the presence of wind derivatives in order to extract energy. The optimal trajectories for energy extraction in the form of neutral energy cycles in the presence of wind gradients were investigated by Zhao [10] and, more recently, Bonnin et al. [11]. Exceptionally complicated urban spaces pose a challenge for the autonomous operation of UAVs. In the urban environment, the characteristic scale is on the order of few meters, which is due to a complex interaction between buildings, trees, and the living world. A simulation tool that captures the unsteady aerodynamics of flight through such a complex terrain has been presented and demonstrated by Cybyk et al. [12]. All strategies previously described omit the advance knowledge or prediction of a wind velocity field ahead of the UAV. However, a method for sensing flow disturbances in front of miniature UAVs and using the output signal for further control has been demonstrated by Mohamed et al. [13–15]. The control strategy has been developed for roll axis as the most sensitive to wind turbulence. Recent experiments by Watkins et al. [16] related to the measurements of wind vector components on several spanwise locations confirmed a statement about the spatial variation of turbulence magnitude. A flush air data system intended for wind vector sensing in dynamic soaring UAVs was presented by Quindlen and Langelaan [17]. The system used pressure holes on the aircraft nose cone as inspiration from wandering albatross and giant petrel nostrils. An overall view on biologically inspired soaring techniques and aerodynamic structures was illustrated by Rasuo [18].

Being three-dimensional, turbulence scales larger than wingspan would result in only the pitching attitude of the aircraft. However, a case of turbulence smaller than wingspan leads to unequal lift distribution and a need for control of the oncoming roll and yaw moment. A method for the atmospheric disturbance effect on roll and yaw motions has been proposed by Ringnes and Frost [19] based on well-known Prandtl lifting-line theory. Moreover, besides the already described methods of gust energy extraction using active control, some benefits could be achieved using a passive approach that makes use of the longitudinal stability of the aircraft and the dynamic response of the structure, particularly of the wing by Ironside et al. [20,21] and Mai [22].

III. Wind Model

All the disturbances present on Earth or even far away can contribute to wind formations. Either unequal heating of the ground provoked by the clouds or natural obstacles such as cliffs, mountains, and valleys (or even sea currents) are provoking uneven pressure fields that drive the motion of air. Besides low altitude, UAVs usually fly in urban environments surrounded by buildings, trees, and other obstacles, where the characteristic scale is on the order of a few meters. Such a complex surrounding implies intricate interaction between the terrain geometry, physical conditions, and varying meteorology. It is well known that, with increasing closeness to the ground, the turbulence intensity increases and changes characteristics. Above the atmospheric boundary layer, the air is relatively smooth. At heights relevant to military and commercial aircraft operations, we have clear turbulence and turbulence due to convection, but this is not relevant here. From field experiments, it is well known that undisturbed wind velocity is variable in space, time, and direction. A model of the turbulent wind field suitable for calculations requires good representation of both the temporal and spatial structures of turbulence. The most adequate method to simulate a turbulent wind field would be to solve Navier–Stokes equations of an atmospheric flow bounded from below by an aerodynamically rough surface. However, the computational cost would be enormous. An alternative could be large-eddy simulations as an approximate solution to the Navier–Stokes equations, where the smallest scales are not solved directly but modeled. Still, even simplified alternatives require significant computational power. Therefore, empirical description is generally used for turbulent flight using spectral and coherence descriptions of turbulence.

A general algorithm to simulate the three-dimensional field of three components of wind velocity fluctuations was developed by Mann [23,24]. The method built a model of a spectral tensor for representation of atmospheric turbulent boundary layer. It led to a natural representation of three-dimensional turbulent flow of less computational cost as compared to the alternative large-eddy simulation or Navier–Stokes equations. Widely used Dryden and von Kármán spectral representations describe an average of all conditions for clear air turbulence. The limitations for those two models are due to the factors not incorporated into the spectral representation, such as terrain roughness, wind shear, and mean wind magnitude. On the contrary, Kaimal and Finnigan's spectra were developed on measurements over flat homogeneous terrain [25]. The main finding of Kaimal and Finnigan[25] was the jump in spectral energy density at low frequencies as the stability of the atmosphere changed from stable (cooling from below) to unstable (warming from below) according to Mann [23]. The recent findings of Fortuniak and Pawlak [26] confirmed that, in spite of some differences, the spectral and cospectral properties of the flow at the top of the urban roughness sublayer were very similar to those for homogeneous flat terrain, and many universal functions found for such surfaces can be directly applied over urbanized areas. It was also found that the analytical model of the neutral spectrum in the entire frequency range given by Kaimal and Finnigan [25] fit quite well the urban data in the case of the vertical wind component. The spectrum used in the simulation

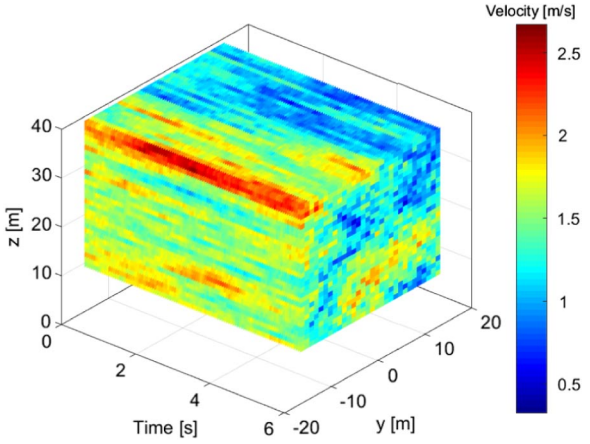

a) Velocity magnitude in generated wind field

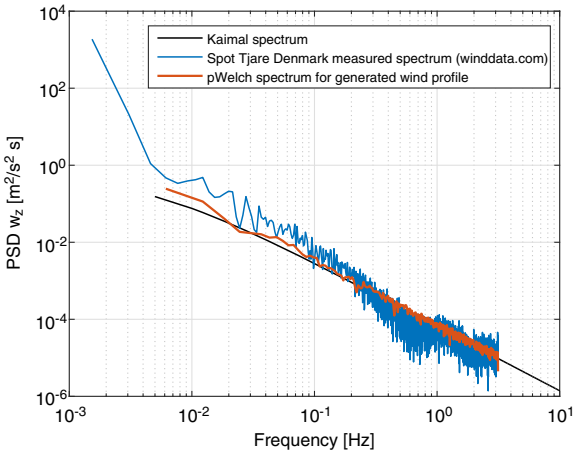

b) Power spectral density (PSD) of generated time series and measurements

Fig. 1 Three-dimensional wind field.

was presented by Kaimal and Finnigan [25], where $\alpha = w_x, w_y, w_z$; and A and B were adjustable constants that depended on the chosen length scales. The method for the generation of a single wind time series from a Kaimal and Finnigan spectrum was proposed by Branlard [27]. The generated wind field shown in Fig. 1a provided a three-dimensional grid of desired spatial resolution, which will be used later as an environment of flight for gust energy extraction.

The characteristics of the generated profile are compared with an available database on wind characteristics [28], which provides overall information of the wind measured at various mast heights near the wind turbine stations at many places in the world. The reference locations for turbulence energy were the Tjare spot in Denmark (described as pastoral, flat landscape) and San Gorgonio in United States (with rolling hills covered with bushes and small trees). The corresponding reference wind profiles were taken at the mast heights of 30 and 40 m of altitude. These profiles are the reference for parameters of Kaimal and Finnigan [25] spectral formulation in order to generate a wind field as close as possible to reality (see Fig. 1b for spectral representation):

$$F_\alpha(k_1) = \frac{A\sigma_u^2/k_{wm}}{1 + B(k_w/k_{wm})^{5/3}} \tag{1}$$

The key parameters associated with external flows that drive the urban environment include the following parameters according to Cybyk et al. [12]: intensity of turbulence, turbulence length scales, surface roughness, Reynolds number, and Richardson number.

IV. Flight Dynamics

Here, we reveal the system of differential equations that describes the physics of flight in a gusty environment. The first derivation of equations is done for the longitudinal plane. Also, some efforts are exposed in order to reveal dynamic energy transfer between the aircraft and wind. First, the simulations are performed with a sinusoidal vertical velocity wind profile for various frequencies, taking into account the unsteady behavior of the aircraft. Second, a more realistic multipoint model has been constructed for flight within a three-dimensional wind field, considering the influence of all the unsteadiness that it brings. Both flight cases are done with an active control of proportional gains that were optimized for a certain wind scenario. Two methods for unsteady derivative estimation have been proposed and compared. The overall influence of unsteady effects on energy transfer between the atmosphere and aircraft has been determined.

A. Energy Extraction in Longitudinal Plane

Here, we consider only the longitudinal motion of the aircraft represented as point mass model as shown in Fig. 2. The derivation of the equations follows the previous works of Langelaan [6,7] and Lawrence and Sukkarieh [9]. The influence of wind gradients on the overall power of the aircraft in the function of the climb angle have been done by Lawrence and Sukkarieh [9]. It is clear that an aircraft has to perform certain maneuvers according to the knowledge of the velocity field and the control strategy in order to increase their power, absorbing the energy from the atmosphere. The kinematics of the aircraft is solved with the Runge–Kutta ordinary differential equations solver ODE45 found in MATLAB. The solutions of the system are velocity, climb, and flight-path angle, from which all other parameters of flight can be evaluated:

$$T - D - W\sin\gamma = \frac{W}{g}(\dot{V} + \dot{w}_x\cos\gamma - \dot{w}_z\sin\gamma) \tag{2}$$

$$-L + W\cos\gamma = \frac{W}{g}(-V\dot{\gamma} + \dot{w}_x\sin\gamma + \dot{w}_z\cos\gamma) \tag{3}$$

$$M = \ddot{\theta} I_{yy} \tag{4}$$

The main objective of gust soaring is to increase the energy state of the aircraft by performing certain maneuvers according to the current wind velocity perturbations. Energy gain can also be achieved with optimal climb for the negative component of vertical wind velocity, which is known as updraft and exploited by all glider pilots in thermals. Another way is through active control according to the setting of wind derivatives:

$$\frac{\dot{E}_a}{m} = -g w_z + \frac{qS}{m}(C_T - C_D)V - V(\dot{w}_x\cos\gamma - \dot{w}_z\sin\gamma) \tag{5}$$

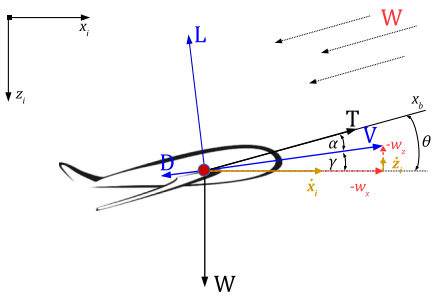

Fig. 2 Two-dimensional flight physics of mass point model.

The control used in this work is based on a set of proportional gains, which has been previously demonstrated by Langelaan [6]. Simply, aircraft will react according to input information of the a priori known wind by flaps or a horizontal tail. It should be pointed out that the gains have to be optimized with certain sensitivity to the magnitude of the wind. Once obtained values for a certain wind profile will not be optimal for others with higher frequency and magnitude. This is due to the fact that every reaction has to outweigh the drag increase in the specific power equation:

$$\delta = \begin{bmatrix} \delta_e \\ \delta_f \end{bmatrix}, \quad \text{where } \delta_e = \begin{bmatrix} k_1 w_z \\ k_2 w_x \\ k_3 \dot{w}_x \\ k_4 \dot{w}_z \end{bmatrix} \quad \text{and} \quad \delta_f = \begin{bmatrix} k_5 w_z \\ k_6 w_x \\ k_7 \dot{w}_x \\ k_8 \dot{w}_z \end{bmatrix} \tag{6}$$

Wind velocity in a two-dimensional model has been modeled as a sinusoidal function. In this way, we are able to recognize more obviously the response of the aircraft and involve potentially beneficial unsteady effects, depending on the frequency of posed wind profile:

$$w_z = k_g \sin(\omega_g t) \quad \text{and} \quad \dot{w}_z = k_g \omega_g \cos(\omega_g t) \tag{7}$$

The term endurance is usually related to a constant value, which is very often calculated for steady flight and represents the ratio of available energy and power required. In the case of steady flight, those parameters are quite obvious because the velocity and altitude can be assumed constant. However, in flights through gusty wind, the objective is to gain energy with time, thus increasing the specific power during the flight path. The benefit in endurance could be evaluated according to the following:

$$\frac{\Delta E_t}{E_t} = \int_0^t \left(1 - \frac{P}{P_c}\right) \mathrm{d}t \tag{8}$$

The equation claims that, by increasing the specific power with control P_c (where P is the power during the flight without energy harvesting control), we increase the magnitude of ΔE_t, thus increasing the energy state.

1. Dynamic Energy Transfer Between Wind and Aircraft

The goal is understanding of energy harvesting mechanisms through equations of motion and the possible influence of some aerodynamic parameters. The flight of the airplane is considered to be symmetric, and wind disturbances are coming from a vertical plane. Once again, the power equation can be transformed now, revealing a new aerodynamic parameter as shown in following equation:

$$\frac{\dot{E}_a}{m} = -g w_z - g\sqrt{\frac{2n^3}{\rho}\frac{W}{S}}\left(\frac{C_D}{C_L^{3/2}}\right) - V(\dot{w}_x \cos\gamma - \dot{w}_z \sin\gamma) \tag{9}$$

The second term (representing the power required) claims that the maximum energy transfer between the wind and the aircraft will be achieved at a maximum value of the factor $C_L^{3/2}/C_D$ (corresponding to the minimum sinking rate) for both stationary ($n = 1$) and nonstationary flights ($n \neq 1$). The term accounts as power required and should be minimized, allowing higher levels of gained energy from wind power terms. It is also well known that, in case of thermals (assuming stationary updraft), the glider pilot should determine the speed to fly based on the strength of the next thermal according to the MacCready theory.

Further integration of the wind power part reveals specific cases in which energy transfer can be maximized. It is obvious that the presence of a negative vertical wind component (updraft) increases the energy state of the aircraft. On the other hand, considering wind derivatives in the longitudinal plane, we can differentiate some specific flight cases for maximization of energy transfer. Those specific flight cases for energy maximization have been obtained, with detailed decomposition involving first- and second-order derivations of power equation parts related to the wind:

$$\frac{\dot{E}_{a,\dot{w}_x}}{m} = -V\dot{w}_x \cos\gamma = -\frac{\partial w_x}{\partial x}(V\cos\gamma + w_x)V\cos\gamma - \frac{\partial w_x}{\partial z}(-V\sin\gamma + w_z)V\cos\gamma \tag{10}$$

$$\frac{\dot{E}_{a,\dot{w}_z}}{m} = V\dot{w}_z \sin\gamma = \frac{\partial w_z}{\partial x}(V\cos\gamma + w_x)V\sin\gamma + \frac{\partial w_z}{\partial z}(-V\sin\gamma + w_z)V\sin\gamma \tag{11}$$

Isolation of different wind parts and multiple derivations bring the following extremes, for which corresponding flight cases are illustrated in Fig. 3:

1) Climbing/descending into positive/negative wind shear $\partial w_x/\partial z$ would increase the specific power of the aircraft where positive/negative horizontal wind shear would imply an optimal angle:

$$\gamma = \sin^{-1}\frac{w_z \pm \sqrt{8V^2 + w_z^2}}{4V}$$

2) An optimal soaring strategy for power maximization in the case of positive/negative vertical wind shear $\partial w_z/\partial x$ would be climb/descent for an optimal climb/descent angle:

$$\gamma = \cos^{-1}\frac{w_x \pm \sqrt{8V^2 + w_x^2}}{4V}$$

3) For a positive/negative linear vertical wind, a gradient optimal climb angle would be

$$\gamma = \sin^{-1}\frac{w_z}{2V}/\text{maximum climbing angle}$$

Note that the previous equations are developed with respect to the air-path system. On the other hand, the final form of the power equation for the inertial system is as follows:

$$\frac{\dot{E}_i}{m} = -q\frac{S}{m}C_D(V + w_x\cos\gamma - w_z\sin\gamma) - q\frac{S}{m}C_L(w_x\sin\gamma + w_z\cos\gamma) \tag{12}$$

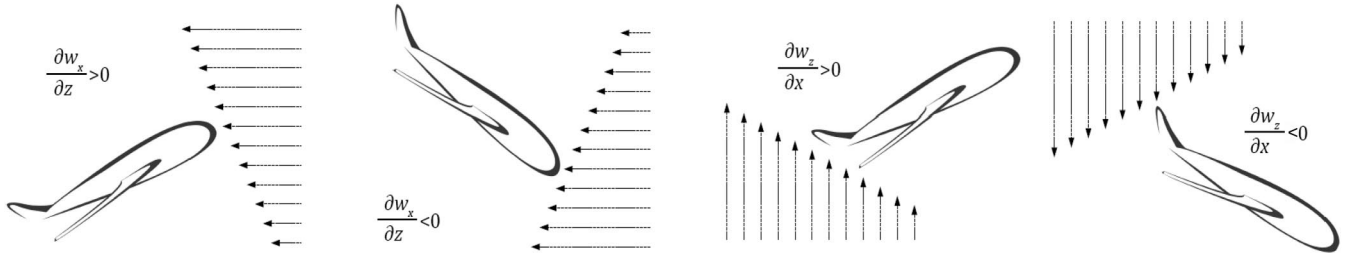

Fig. 3 Flight cases for specific power maximization in wind shear (maximum specific power in wind shear is obtained for $\gamma = \pm 45$ deg).

Wind gradients do not appear explicitly in the expression for the total power expressed with respect to the inertial frame. However, time- and spatially varying winds will result in time-varying forces (through changes in airspeed and angle of attack), so wind gradients will indirectly affect total power.

B. Multipoint Model for Energy Harvesting

To approach a flight strategy in a gusty environment with a more realistic flight scenario, by introducing three-dimensional effects, a multipoint model has been developed. The model consisted of three points representing two wind sensors on the wing and a central mass point (see Fig. 4). Because all points travel in a space grid of wind, trilinear interpolation [29] is applied, taking into account all surrounding seed points of the mesh. This would provide an alternative case of simulation to a real flight test with equipped multihole probes capable of measuring three wind velocity components, as has been demonstrated by Mohamed et al. [13]. A multipoint model allows estimation of an unequal lift and drag distribution at each side of the wing, allowing instantaneous knowledge of the necessary control action for the coupling of roll and yaw moments. It also provides the information of the gust length scale, frequency, and magnitude, on which can be based teh control strategy of the real flight, evading unnecessary actions in the case of small length scales. The equations of motion are based on the mathematical model presented by Rasuo [30] and expanded, taking into account lateral and roll motions with wind components. A system of differential equations is once again integrated numerically using a Runge–Kutta ODE45 solver with an adapted time step to the wind velocity field:

$$T - D - W\sin\gamma = \frac{W}{g}(\dot{V} + \dot{w}_x\cos\psi\cos\gamma + \dot{w}_y\sin\psi\cos\gamma - \dot{w}_z\sin\gamma) \tag{13}$$

$$L - W\cos\gamma = \frac{W}{g}(-V\dot{\gamma} + \dot{w}_x\cos\psi\sin\gamma + \dot{w}_y\sin\psi\sin\gamma + \dot{w}_z\cos\gamma) \tag{14}$$

$$L\sin\phi = \frac{W}{g}(V\dot{\psi}\cos\gamma - \dot{w}_x\sin\psi + \dot{w}_y\cos\psi) \tag{15}$$

The model assumes that the roll rate is directly controlled as a response from the unequal angle of attack along the wingspan. The two side points move according to the rotation of the aircraft angle ψ and emulate wing sensors as, for example, multihole probes. The information on wind velocity is then transformed into additional velocity and angle of attack, seen by each side of the wing. The corresponding roll and yaw moment are then estimated with a lifting-line theory that was demonstrated by Ringnes and Frost [19]:

$$\frac{\dot{E}_a}{m} = -gw_z + \frac{qS}{m}(C_T - C_D)V - V(\dot{w}_x\cos\psi\cos\gamma + \dot{w}_y\sin\psi\cos\gamma - \dot{w}_z\sin\gamma) \tag{16}$$

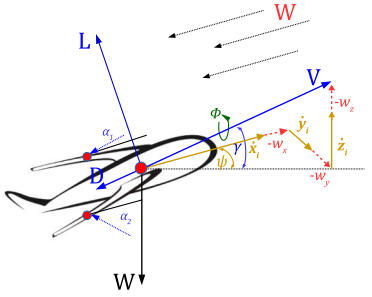

Fig. 4 Three-dimensional flight physics of multipoint mass model.

The control strategy has remained the same as for the longitudinal case. Once again, the optimization of control gains has to be performed with the aim to increase the energy state of the aircraft. Time histories of the roll and yaw moment are showing the moment acting on a wing that would be lost if no spanwise variation in turbulence was assumed. These moments are referred as added, and they are expressed as follows:

$$M_{\text{roll},a} = \int_{-b/2}^{b/2} l(y)y\,\mathrm{d}y \tag{17}$$

$$M_{\text{yaw},a} = \int_{-b/2}^{b/2} d_i(y)y\,\mathrm{d}y \tag{18}$$

where $l(y)$ and $d_i(y)$ are the sectional lift and induced drag as functions of spanwise location y.

C. Unsteady Aerodynamics

Generally, the aircraft's lift and pitch moment coefficients can be represented by the MacLaurent series according to Stojakovic and Rasuo [31] with the following expressions:

$$C_L = C_{L0} + C_{L\alpha}\alpha + C_{L\dot{\alpha}}\frac{\dot{\alpha}l}{2V} + C_{L\dot{\theta}}\frac{\dot{\theta}l}{2V} + C_{L\ddot{\alpha}}\frac{\ddot{\alpha}l^2}{4V^2} + \sum_{\text{Control}}\left(C_{L\delta}\delta + C_{L\dot{\delta}}\frac{\dot{\delta}l}{2V} + \dots\right) + \dots \tag{19}$$

$$C_M = C_{M0} + C_{M\alpha}\alpha + C_{M\dot{\alpha}}\frac{\dot{\alpha}l}{2V} + C_{M\dot{\theta}}\frac{\dot{\theta}l}{2V} + C_{M\ddot{\alpha}}\frac{\ddot{\alpha}l^2}{4V^2} + \sum_{\text{Control}}\left(C_{M\delta}\delta + C_{M\dot{\delta}}\frac{\dot{\delta}l}{2V} + \dots\right) + \dots \tag{20}$$

Aerodynamic derivatives can be divided in two groups. The first group can be obtained by steady methods such as, for example, the modified vortex lattice method with included viscous effects; whereas the other has to involve unsteady effects proposed in the following section.

Driven by the nature of turbulence, the control activation is of high frequencies. Therefore, aircraft will perform rapid maneuvers followed by the violent variation in angle of attack. Depending on the frequency and magnitude of the pitching and heaving motion, trailing vortices are generated, introducing unsteady behavior of the aerodynamic forces. Theodorsen [32] modeling of an aeroelastic airfoil was published back in 1935, where aerodynamic forces were represented as a sum of noncirculatory and circulatory effects for a thin section:

$$L = L_{\text{nc}} - 2\pi\rho VbJ(k)\omega(t) \tag{21}$$

The transfer function $J(k)$ transforms a quasi-steady prediction of circulatory aerodynamic forces to unsteady values, introducing a time lag effect. Because we are dealing with time domain variations, an inverse Fourier transformation is applied for Wagner functions approximated by Jones [33]. Those functions are also available for several aspect ratios, which enables comparison for various wing dimensions. The complete system of equations for a nonlinear response of a typical airfoil section exposed in the state-space formulation was done by Kholodar and Dowell [34].

An alternative way for the estimation of unsteady derivatives was recently proposed by Gili et al. [35]. It involved an unsteady Reynolds-averaged Navier–Stokes equation solver coupled with rigid-body motion available in the STAR-CCM+ software package. The attractive side of this method was that there was no need for a remeshing, deformable, or interface mesh, which is highly cost effective in terms of time. The domain was the same as for steady computations with an imposed motion law. The tested airfoil is

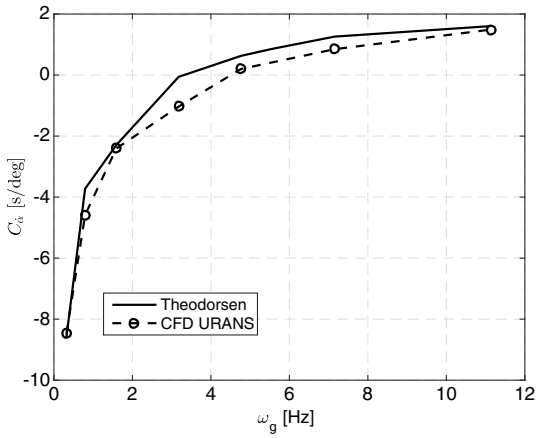

a) Unsteady derivative $C_{\dot{\alpha}}$ for harmonic pitch

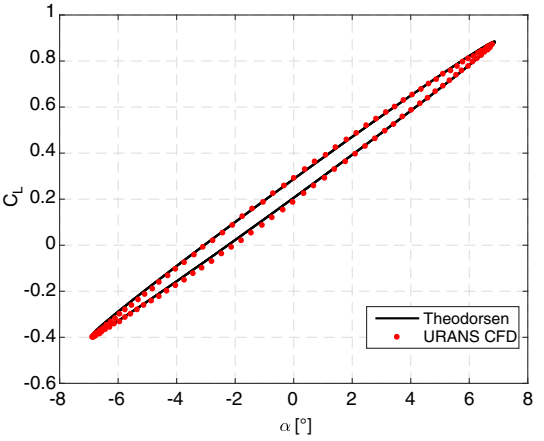

b) Lift coefficient for harmonic pitch with amplitude of 6.8 deg and frequency of 1.6 Hz; reduced frequency k = 0.075

Fig. 5 Unsteady derivative estimation comparison between Theodorsen and unsteady Reynolds-averaged Navier–Stokes (URANS) simulations.

SD2048, which belongs to the family of low-Reynolds-number foils. A structured hexahedral mesh has been constructed with refined boundary-layer modeling, and number of elements have been chosen based on convergence criteria. The time step chosen for unsteady simulations is of the order 0.5×10^{-4} s. Because the Theodorsen model was developed for flat plate, certain modifications had to be done for adequate comparison with the airfoil. To fit the curves of the resulting lift coefficient, the translation for C_{Lo} and rotation for $C_{L\alpha}$ obtained from steady simulation had to be implemented for the theoretical model of Theodorsen. After the implementation of corrections, a certain gap in the lift slope was found due to the viscous effects modeled by computational fluid dynamics (CFD). Nevertheless, am acceptable comparison has been found, both for the harmonic pitch and coupled motion of pitch and heave. Note that Fig 5b illustrates the lift coefficient with a reduced frequency greater than 0.05. The unsteady derivative coefficients have been taken for simulations where flow is considered unsteady ($k > 0.05$). For a flight with an airspeed of 18 m/s and a cord of 0.27 m, the oscillations in α with a frequency greater than 1.1 Hz should be considered with unsteady aerodynamics.

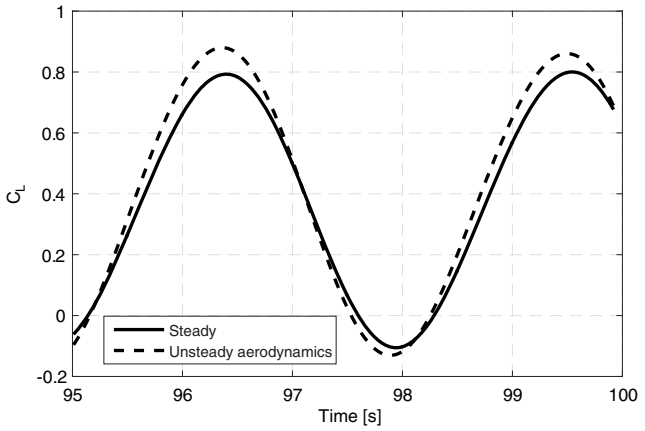

Fig. 6 Unsteady vs steady cycle during sinusoidal vertical gust.

The previous effort was realized in order to model a realistic case of lift evolution during energy transfer between the atmosphere and aircraft, followed by aggressive maneuvers. For rapid maneuvers, it is important to include added-mass terms to account for the reaction force due to the mass of the fluid that is accelerated by the airfoil. Additionally, one must include induced circulation around the airfoil due to wake vorticity. Moreover, the importance of taking into account unsteady effects has been justified with improved harvesting cycles. Implemented unsteady derivative coefficients featuring time lag result in an increased lift coefficient (as shown in Fig. 6) during harvesting cycles. Following large accelerations,

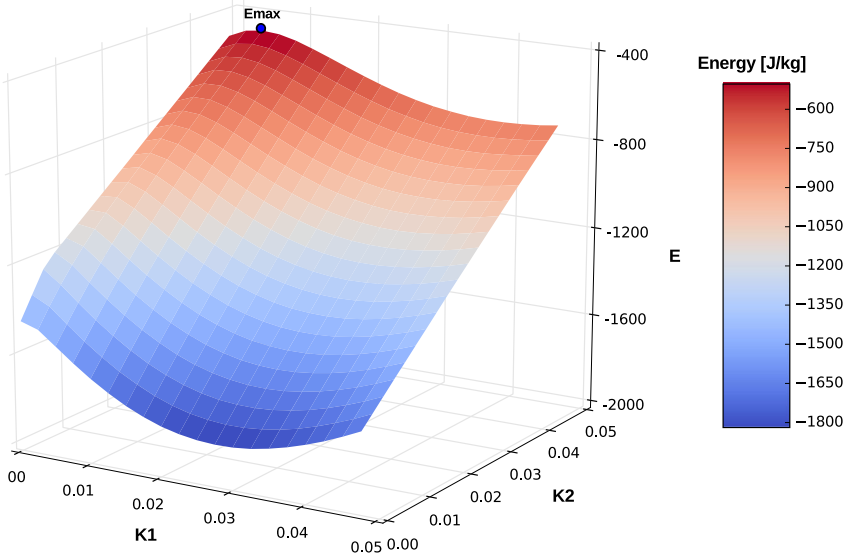

Fig. 7 Optimization topology for sinusoidal gust: $w_z = 2\sin(2t)$.

the lift coefficient is strongly influenced by added-mass forces according to Brunton and Rowley [36]. Those increments can bring additional positive work on aircraft, in comparison to the steady model, increasing harvested energy. Also, it should be pointed out that the frequency response is qualitatively in relation to the position of the rotating point. If the location of the rotation point goes behind the midchord, the effect of added mass with higher frequencies becomes negative. With a positive step in the angle of attack, the lift would move in a negative direction due to the negative added-mass value outperforming circulatory forces.

V. Results

The results have been divided into two groups. The first group is dealing with sinusoidal profiles in the longitudinal plane. In addition, one more profile has been built as a sum of sinusoidal profiles where

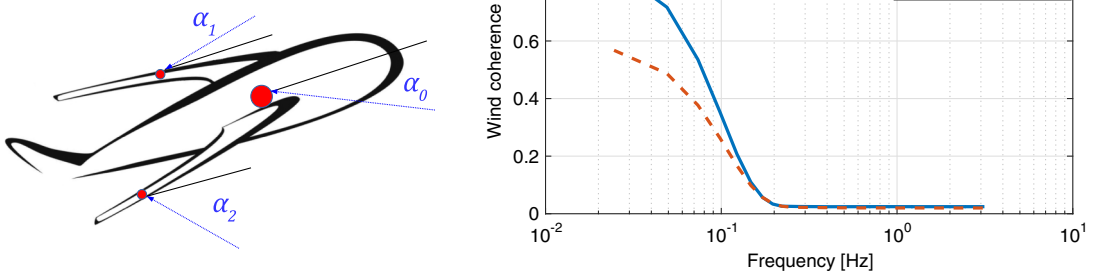

a) Multipoint aircraft system

b) Coherence for wing points 1 and 2 during flight

Fig. 8 Three-dimensional flight.

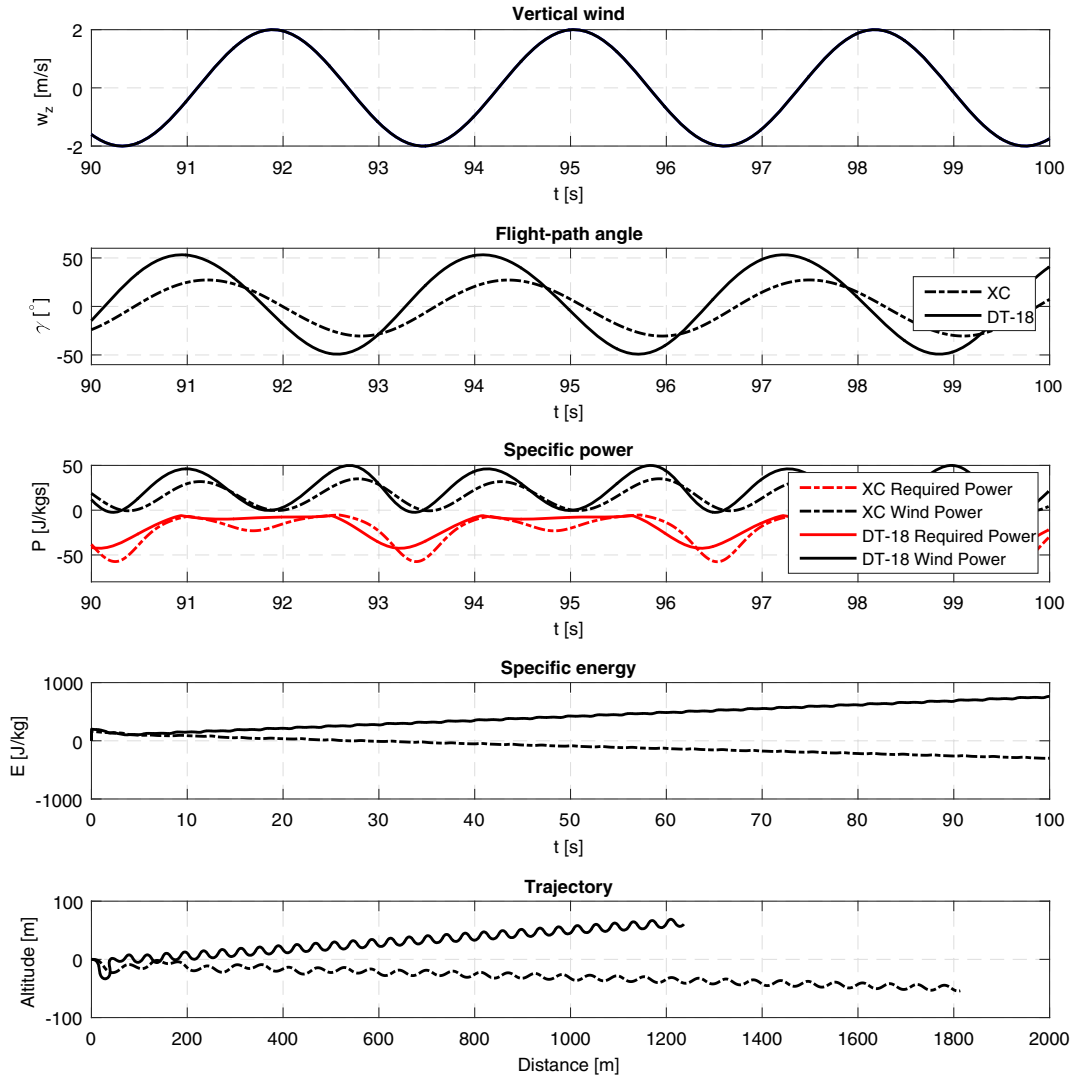

Fig. 9 Longitudinal gliding flight with active control for energy harvesting of XC glider and DT-18 for high-amplitude low-frequency gust: $w_z = 2\sin(2t)$.

frequencies and magnitudes are taken from a Fourier transformation of the realistic profile. Each simulation required optimization of control gains for energy state maximization as shown in Fig. 7. The second group is dealing with a flight through a complex, stochastic, and three-dimensional wind field. In addition, the influence of nonuniform gust distribution along wingspan has been taken into account in the form of supplementary moments and forces generated at different wing locations (See Fig. 8a for multi-point aircraft system). The level of coherence between wing points during flight has been shown in Fig. 8b.

A. Longitudinal Simulation Results

Simulations in the vertical plane have been performed with an imposed sinusoidal wind field characterized with frequency and amplitude, shown in Figs. 9 and 10. Two flight cases for the same gust scenario have been examined: one with active control of proportional gains, and the other without control. Unsteady derivatives have been chosen according to the frequency of the imposed wind field. The values of proportional gains have been optimized for one frequency and magnitude of the presented flight case. Negative unsteady derivative values were shown to have a positive impact on energy harvesting up to a frequency where they changed sign into the positive. Also, it should be pointed out that the optimized gains were not any more optimal for a different frequency or magnitude, which implies a different control strategy in the case of a real flight test.

We differentiate two flights through the sinusoidal vertical wind profile. The first flight is performed with a high-amplitude and low-frequency gust (see Fig. 9), whereas the other flight is performed with a low-amplitude and high-frequency gust (see Fig. 10). The amplitude and frequency were chosen with the aim of having a clear discrepancy between the two profiles while still maintaining the values on a reasonable level. The goal was to identify which frequency and amplitude would be more beneficial in terms of the specific power increase during the energy extraction flight. It was found that, with a higher frequency and lower amplitude, the gust energy extraction required implementation of the regulator and thrust. The regulator and constant-thrust coefficient will maintain aircraft oscillations in γ around the zero axis, which is in correlation with the maximization of energy extraction according to the equations presented in Sec. IV. The gains and coefficients of control for such a flight were optimized using the nonsorting genetic algorithm II (NSGA II) from the OpenMDAO package in PYTHON. The results have shown that energy extraction is possible even from such a small turbulent structure (see Fig. 10 for positive power coming from the wind). However, the amount of thrust needed is greater as compared to the thrust needed for straight regulated flight due to the increased required power. It means that we are consuming more energy

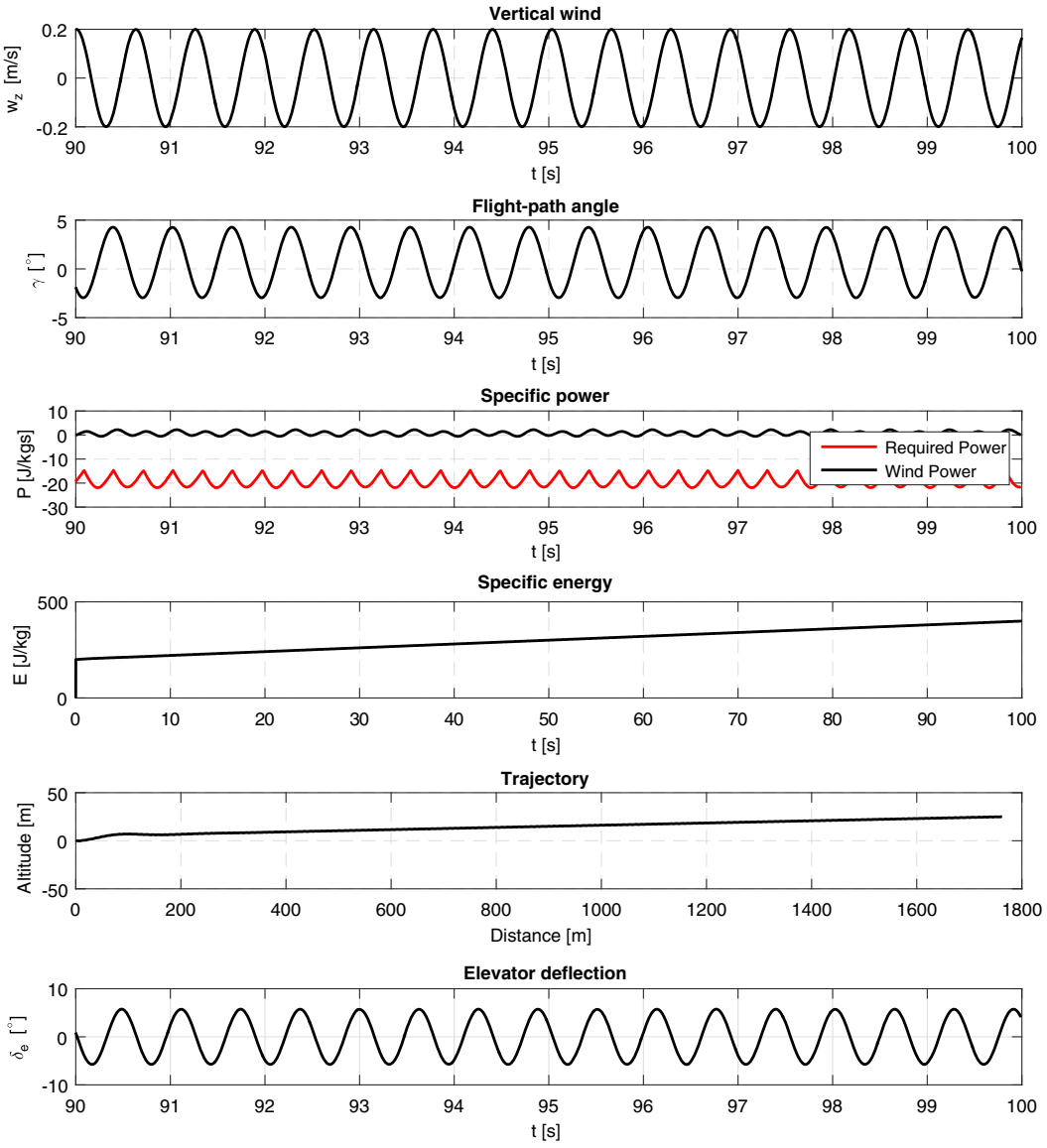

Fig. 10 Longitudinal powered flight with active control and regulator for low-amplitude high-frequency gust: $w_z = 0.2\sin(10t)$.

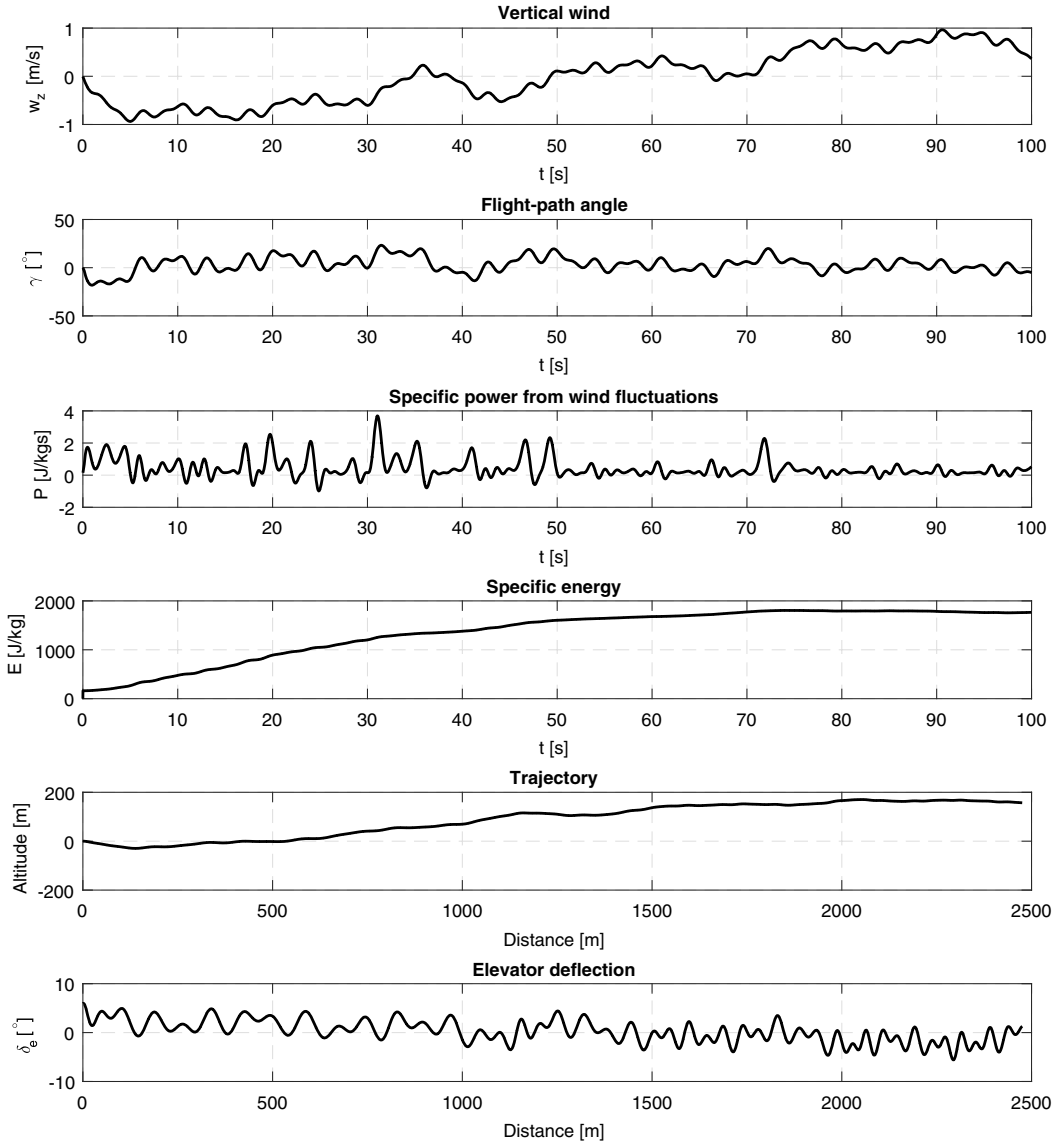

Fig. 11 Flight parameters of longitudinal powered flight for energy extraction from wind fluctuations of filtered realistic wind profile.

for flying in a desired way than we are actually harvesting from the turbulence. In contrast, the case of high-amplitude gust has enough energy coming from the wind to ensure a significant amount of energy gained, even without thrust. The control in the case of high-frequency low-amplitude vertical gust is as follows:

$$\delta_e = k_1 w_z + k_2 \dot{w}_z + k_3 \gamma \quad (\text{with constant} \quad C_T) \tag{22}$$

Moreover, control has been optimized for a flight within a filtered realistic profile in order to quantify the benefit from wind fluctuations (see Fig. 11). Besides the fact that the aircraft is maintaining a mostly positive power contribution from fluctuations, there is a significant growth in power required for such a flight. Achieving positive power from high-frequency wind fluctuations requires rapid maneuvers, which imply significant energy necessary to perform flight.

Two different aircraft served as aerodynamic model for simulations. On the one hand, the XC Bubble Dancer (XC-BD) has twice the wingspan of the DT-18, a higher lift-to-drag ratio, and a higher mass; whereas on the other side, the DT-18 has higher control efficiency (see the appendices for aircraft properties). The results show an evident energy gain (see Fig. 9) for both vehicles. It is interesting to notice that the XC-BD is more aerodynamically efficient because of the higher lift-to-drag ratio, and it achieves a higher level of energy after 100 s of flight. However, in the case of DT-18 flight, energy harvesting is on a higher magnitude by 15%. One of the missions of this paper iss to detect which aerodynamic parameters would contribute to such a difference in energy gain. For that purpose, the equations of motion have been solved with an imposed change of the flight-path angle and an angle of attack for energy state maximization.

One of the parameters recognized for the strong influence on energy harvesting was certainly the lift slope coefficient $C_{L\alpha}$. It was found out that a 10% higher value of lift slope brought 15% more wind power, and the opposite was found for lower values. Another

Table 1 Optimization constraints: parameters of control gains optimization

Parameter	Value
Optimization objective: specific power from wind	Maximize
Velocity V range	[10:30 m/s]
Initial V	18 m/s
Angle-of-attack α no-stall range	[−6:12 deg]
Flight-path angle γ range	[−50:50 deg]
Parameters	$k_1, k_2, \ldots, k_n$
Thrust coefficient for powered flight c_T	[0:0.1]
Optimization package OpenMDAO with 100 generations for NSGA II	— —
SLSQP algorithm with defined Jacobian matrix	— —

affecting parameter is the control effectiveness represented by the coefficient $C_{L\delta_e}$. A more efficient elevator of 25% in comparison to the original plane would bring 8% more average wind power.

The optimal definition of the previously mentioned parameters should be objective in the process of UAV design for energy extraction and long-endurance flight. They indicate how important effective gain

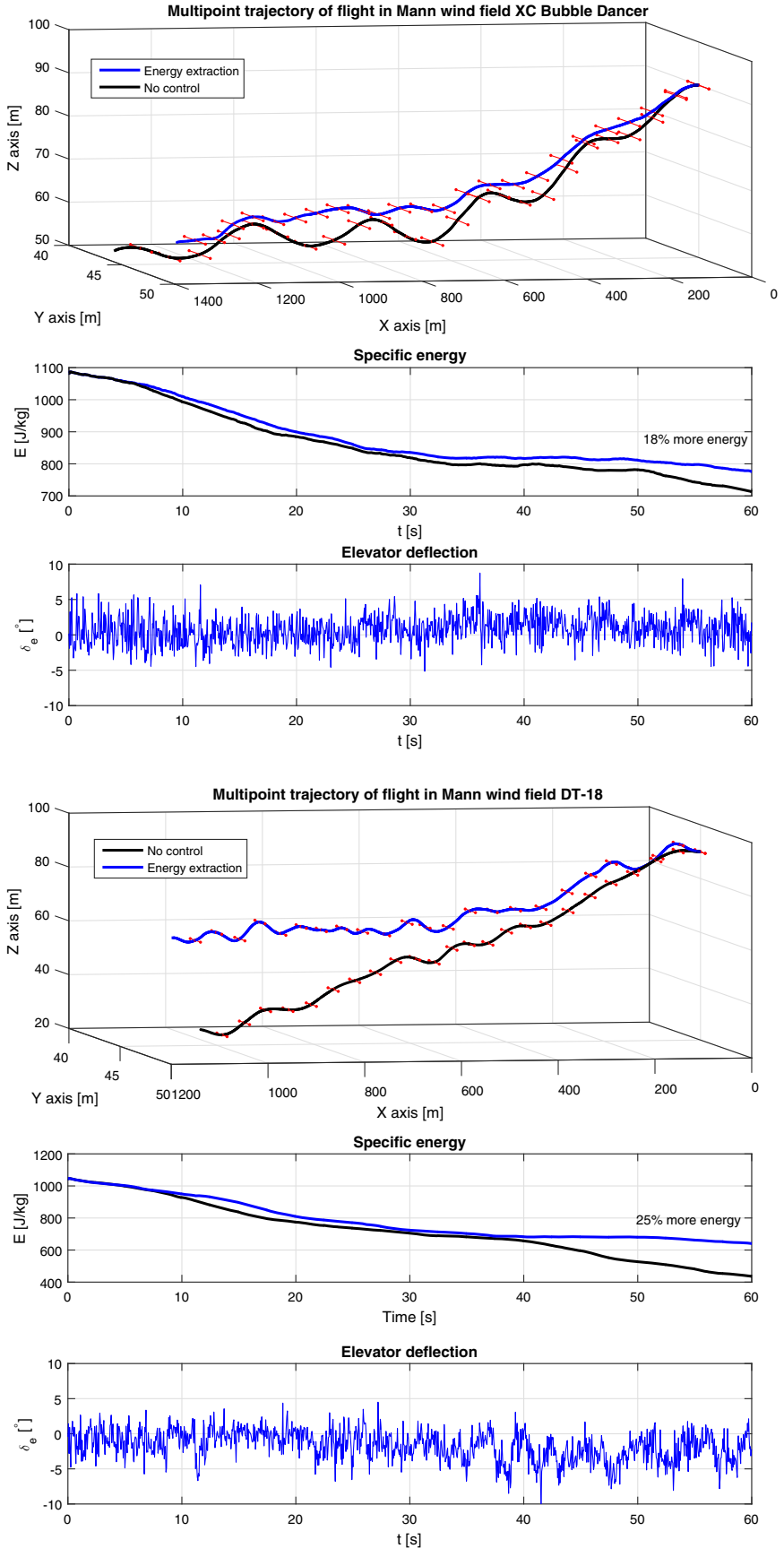

Fig. 12 Trajectory and energy of three-dimensional gliding flight for XC glider and DT-18 through wind box.

is in lift during maneuvering flight within the energy harvesting cycles. As usual, drag reduction is highly beneficial because it directly affects the power required, thus reducing the necessary thrust coefficient for flight. Gaining energy with gust soaring is a constant battle between beneficial part of wind components and the drag increment due to reaction, as described by the power equation.

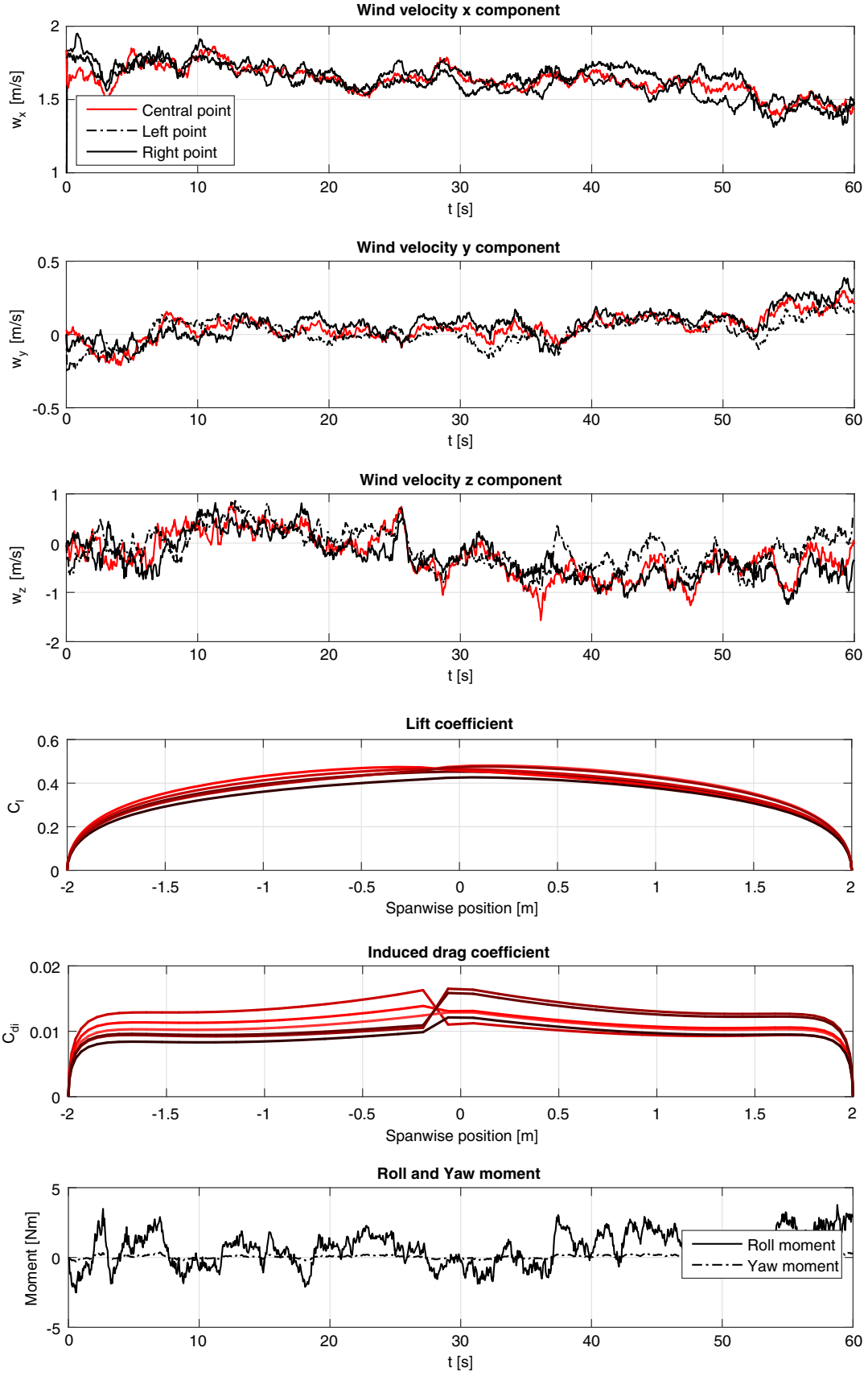

Fig. 13 Roll and yaw moment estimations of XC Bubble Dancer for three-dimensional gliding flight.

1. Optimization of Control Gains

The topology of final energy achieved as a function of the control gains has been built with respect to the constraints of the motion during energy extraction. The optimization problem has been set with the objective function of maximizing the specific power coming from the wind using the nonsorting genetic algorithm II or the sequential least-squares algorithm based on the quasi-Newton method (SLSQP). The optimization constraints are tabulated in Table 1. The control strategy in the presence of only vertical wind characterized as high frequency and low amplitude was based on two control gains, K_1 and K_2, multiplying a priori knowledge of w_z and $\dot{w}_z$, respectively. On the contrary, for low amplitude and high frequency, there were three coefficients and thrust inputs. The case with a horizontal profile would involve two more coefficients, respectively. Despite the fact that the genetic algorithm brings the highest energy harvesting result, the computation time is relatively high. This was important due to the fact that proportional control had to be optimized for each frequency and magnitude of the sinusoidal wind profile, whereas for the case of flight through stochastic wind, gain coefficients were obtained for specific profiles. On the other hand, an attractive algorithm based on the gradient method achieves faster convergence, although it is strongly dependent on the initial values given to the optimizer. With this purpose, a rough topology has been constructed, which is shown in Fig. 7 in order to have more precise idea about the initial values. The difference between the two optimization methods is negligible and goes into favor of the SLSQP method with a proper initiation and Jacobian matrix definition, thus significantly reducing the computational time. Both optimization algorithms included are used in the OpenMDAO package for PYTHON. It was interesting to notice that, while optimizing the control gains for various sinusoidal profiles, the maximum coefficient of lift served as a limiting criteria. More precisely, the gain in specific power would usually be limited by the maximum lift coefficient.

B. Multipoint Three-Dimensional Results

With the aim of a more realistic flight case, three-dimensional flight dynamic simulations have been performed. The flight environment was a three-dimensional wind field of defined spatial and temporal resolution. The vehicle was modeled as a multipoint system, now collecting additional information about the wind velocity from side sensors located on the wing. Based on the assumption that a single point is adequate for an angle-of-attack estimation of the whole wing side, roll and yaw moments are anticipated. The energy harvesting mechanism once again proved to bring significant benefits, even in such a complex wind field, bringing around 20% more energy after 60 s of flight with active control. The trajectory and energy results shown in Fig. 12 confirmed the behavior in longitudinal flight. Once again, the XC plane proved to be more efficient in terms of aerodynamic performance; whereas on the other hand, the DT-18 was more efficient in energy harvesting. Side points that represent wing sensors (e.g., of multihole probes or pressure-based holes on the wing used for the real flight test) are moving according to wing kinematics. The information provided by those points (see Fig. 13) is then transformed into roll and yaw moment provoked by the unequal wind velocity seen by each side of the wing. In the real flight-test campaign, such information would be used for the activation of ailerons and reducing the unwanted actions of the plane. They would also serve as a decisive mechanism triggering reaction for energy harvesting due to the possible unequal length scales of gust.

As artificial flying environment depends on its creator; thus, the coherence level is the subject of definition in a three-dimensional wind field used in this work. It is defined with a specific function described by Saranyasoontorn et al. [37] (see [38] for details):

$$C(r, f) = e^{[-12((fD_r/U_o)^2 + (0.12D_r/L_C)^2)^{0.5}]} \tag{23}$$

The chosen parameters of the previous function result in higher coherence for the horizontal wind component (solid line Fig. 8b) in comparison to the vertical one. This is the reason why we are experiencing more roll than yaw moment in our simulations (shown in Fig. 13), because the lift increment is higher due to the deviations in the angle of attack than in the horizontal velocity.

VI. Conclusions

The data presented demonstrate the feasibility of gust soaring for a small unmanned aerial vehicle (UAV), theoretically quantifying the gain in energy through numerical simulations. The basic system of longitudinal and three-dimensional equations of motion has been derived for flight in the presence of wind. Those equations were further used for development and integration of a power equation. It was shown that, in order to maximize the power coming from the wind, the aircraft needs to use a control that should enable the least possible power required during the flight. On the other hand, for the energy extraction from wind fluctuations, the aircraft needs to follow the oscillations around a zero flight-path angle in order to maximize the power obtained from the wind fluctuations. The energy gain in this case will be directly proportional to the airspeed and magnitude of the flight-path angle achieved according to the wind. It was shown that even low-amplitude fluctuations can be exploited. However, the benefit from those small structures can be overwhelmed by the power required to perform wind energy maximization flight. Therefore, the quantitative benefit from wind fluctuations depends on the aircraft performance capabilities and qualities.

Besides the unrealistic sinusoidal wind profile, although it is easy to manipulate, a complex and stochastic three-dimensional wind field has been used as a flight environment, where realistic wind profiles were used as a reference for artificial three-dimensional wind field generation. A model of unsteady aerodynamics has been implemented in order to simulate the effects provoked by aggressive and rapid maneuvers that are compliant to the stochastic nature of wind. Three-dimensional effects on the wing due to unequal wind experienced along the wingspan have been transformed into roll and yaw moments for the multipoint model. Significant results in energy gain for both of the aircraft analyzed have been recorded, even from such a stochastic wind box.

An inevitable future contribution on the subject of gust energy harvesting would be the definition of the design process according to the relation between the aircraft geometry and energy gain. Of particular interest will be the definition of an optimal design strategy for a UAV that would more effectively extract energy from the gust.

Gust soaring was theoretically proved to be a very promising flight technique for endurance enhancement. However, in order to reach a full understanding about the refined kinematics and energy exchanges, it seems necessary to perform a flight-test campaign including an aircraft equipped with a sophisticated wind measurement system. It would bring requisite knowledge of the real wind length scales and a challenging control strategy.

Appendix A: Aircraft Properties of XC Bubble Dancer

The aircraft model used in the simulations is the XC Bubble dancer (shown in Fig. B1a) designed by Mark Drela. The coefficients presented in Table B1 are obtained with several software packages based on the vortex lattice method. For the sake of comparison and confirmation, we have used a modified version of Mark Drela's Athena Vortex Lattice (AVL) that takes into account viscous effects by interpolating viscous polar information in the function of the Reynolds number of a certain surface section.

Appendix B: Aircraft Properties of DT-18

The commercial multipurpose UAV shown in Fig. B1b made by Delair-Tech (Toulouse, France) is now one more example of lighter class. Before serial production, the wind-tunnel campaign was performed, allowing comparison with any available software for aerodynamic analysis. Estimation of the aerodynamic derivatives and coefficients has been done with a modified version of AVL, including the prediction of viscous drag, where the viscous drag coefficient $c_{\mathrm{vd}} = c_{\mathrm{vd}}(Re, \alpha_t)$ depended on a chord-based Reynolds number and the total angle of attack α_t (see Table B2).

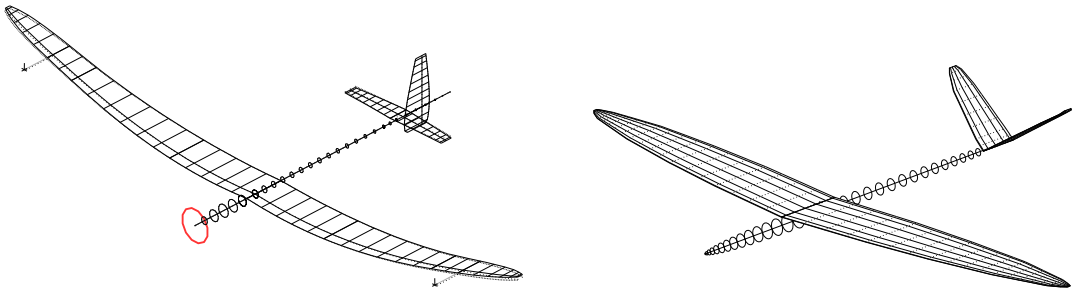

a) XC bubble dancer **b) DT-18**

Fig. B1 Aircraft used in simulations.

Table B1 XC bubble dancer

Aerodynamic properties		
Parameter	Value	Description
M	8 kg	Mass of the aircraft
b	4 m	Wingspan
l_a	0.232 m	Mean aerodynamic cord
S	0.86 m^2	Surface of wing
Airfoil	AG23, AG24, AG26, and AG27	Wing
V	18 m/s	Cruise speed
I_{xx}	1.85 kg $\cdot$ m^2	Roll moment of inertia
I_{yy}	0.684 kg $\cdot$ m^2	Pitch moment of inertia
I_{zz}	2.5 kg $\cdot$ m^2	Yaw moment of inertia
λ	18.836	Wing aspect ratio
$(C_L/C_D)_{\max}$	25	Lift to drag ratio
C_{Lo}	0.35	Lift coefficient for $\alpha = 0$
$C_{L\alpha}$	5.526/rad	Lift slope
C_{Lq}	9.2 s/rad	—
$C_{L\delta_e}$	−0.35/rad	—
$C_{L\delta_f}$	1.58/rad	—
C_D	$5\times10^{-7}\alpha^5 - 3\times10^{-6}\alpha^4 - 5\times10^{-5}\alpha^3 + 1\times10^{-4}\alpha^2 + 5\times10^{-4}\alpha + 0.0186$	Drag coefficient
$C_{D\delta_e}$	0.01/rad	—
$C_{D\delta_f}$	0.035/rad	—
C_{Mq}	−13.56 s/rad	—
$C_{M\alpha}$	−1.21 s/rad	—
$C_{M\delta_e}$	1.48/rad	—

Table B2 DT-18

Aerodynamic properties		
Parameter	Value	Description
M	1.9 kg	Mass of the aircraft
b	1.8 m	Wingspan
l_a	0.18 m	Mean aerodynamic cord
S	0.248 m^2	Surface of wing
V	15 m/s	Cruise speed
I_{xx}	0.184 kg $\cdot$ m^2	Roll moment of inertia
I_{yy}	0.12 kg $\cdot$ m^2	Pitch moment of inertia
I_{zz}	0.66 kg $\cdot$ m^2	Yaw moment of inertia
λ	13	Wing aspect ratio
$(C_L/C_D)_{\max}$	15	Lift to drag ratio
C_{Lo}	0.4	Lift coefficient for $\alpha = 0$
$C_{L\alpha}$	6.37/rad	Lift slope
C_{Lq}	13.9254 s/rad	—
$C_{L\delta_e}$	0.6188/rad	—
$C_{L\delta_f}$	2.158/rad	—
C_D	$C_1\alpha^5 + C_2\alpha^4 + C_3\alpha^3 + C_4\alpha^2 + C_5\alpha + C_6$	Drag coefficient
$C_{D\delta_e}$	0.02292/rad	—
$C_{D\delta_f}$	0.0286/rad	—
C_{Mq}	−24.68 s/rad	—
$C_{M\alpha}$	−3.22 × s/rad	—
$C_{M\delta_e}$	−2.4977/rad	—
$C_{M\delta_f}$	−0.3953/rad	—

References

[1] Scott, D., and McFarland, C., *Bird Feathers—A Guide to North American Species*, Stackpole Books, Mechanicsburg, PA, 2010, pp. 13–41.

[2] Videler, J. J., *Avian Flight*, Oxford Ornithology Series, Oxford Univ. Press, New York, 2005, pp. 46–50.

[3] MacCready, P., "Optimum Airspeed Selector," *Soaring*, Jan.–Feb. 1958, pp. 10–11.

[4] Makovin, D., and Langelaan, J., "Optimal Persistent Surveillance Using Coordinated Soaring," *AIAA Guidance, Navigation and Control Conference*, AIAA Paper 2014-0261, 2014. doi:10.2514/6.2014-0261

[5] Patel, C. K., and Kroo, I., "Control Law Design for Improving UAV Performance Using Wind Turbulence," *AIAA Aerospace Sciences Meeting and Exhibit*, AIAA Paper 2006-0231, 2006. doi:10.2514/6.2006-231

[6] Langelaan, J., "Biologically Inspired Flight Techniques for Small and Micro Unmanned Aerial Vehicles," *AIAA Guidance, Navigation and Controls Conference*, AIAA Paper 2008-6511, 2008. doi:10.2514/6.2008-6511

[7] Langelaan, J., "A Gust Controller for Small Uninhabited Gliders," *Technical Soaring*, Vol. 35, No. 2, 2011, pp. 48–60.

[8] Depenbusch, N., and Langelaan, J., "Receding Horizon Control for Atmospheric Energy Harvesting by Small UAVs," *AIAA Guidance, Navigation and Controls Conference*, AIAA Paper 2010-8180, 2010. doi:10.2514/6.2010-8180

[9] Lawrance, N., and Sukkarieh, S., "Wind Energy Based Path Planning for a Small Gliding Unmanned Aerial Vehicle," *AIAA Guidance, Navigation and Control Conference*, AIAA Paper 2009-6112, 2009. doi:10.2514/6.2009-6112

[10] Zhao, J., "Optimal Patterns of Glider Dynamic Soaring," *Optimal Control Applications and Methods*, Vol. 25, No. 2, 2004, pp. 67–89. doi:10.1002/oca.739

[11] Bonnin, V., Toomer, C., Benard, E., and Moschetta, J. M., "Energy-Harvesting Mechanisms for UAV Flight by Dynamic Soaring," *AIAA Guidance, Navigation and Controls Conference*, AIAA Paper 2013-4841, 2013. doi:10.2514/6.2013-4841

[12] Cybyk, Z., McGrath, E., Frey, M., Drewry, G., Keane, F., and Patnaik, G., "Unsteady Airflows and Their Impact on Small Unmanned Air Systems in Urban Environments," *Journal of Aerospace Information Systems*, Vol. 11, No. 4, 2014, pp. 178–194. doi:10.2514/1.I010000

[13] Mohamed, A., Abdulrahim, M., Watkins, S., and Clothier, R., "Development and Flight Testing of a Turbulence Mitigation System for Micro Air Vehicles," *Journal of Field Robotics*, Vol. 33, No. 5, 2016, pp. 639–660. doi:10.1002/rob.2016.33.issue-5

[14] Mohamed, A., Watkins, S., Fisher, A., Marino, M., Massey, K., and Clothier, R., "A Feasibility Study of Bio-Inspired Wing-Surface Pressure Sensing for Attitude Control of Micro Aerial Vehicles," *Journal of Aircraft*, Vol. 52, No. 3, 2015, pp. 827–838. doi:10.2514/1.C032805

[15] Mohamed, A., Watkins, S., Clothier, R., and Abdulrahim, M., "Influence of Turbulence on MAV Roll Perturbations," *International Journal of Micro Air Vehicles*, Vol. 6, No. 3, 2014, pp. 175–190. doi:10.1260/1756-8293.6.3.175

[16] Watkins, S., Milbank, J., Loxton, B., and Melbourne, W., "Atmospheric Winds and Their Implications for Microair Vehicles," *AIAA Journal*,

Vol. 44, No. 11, 2006, pp. 2591–2600.
doi:10.2514/1.22670

[17] Quindlen, J., and Langelaan, J., "Flush Air Data Sensing for Soaring-Capable UAVs," *AIAA 51st Aerospace Science Meeting*, AIAA Paper 2013-1153, 2013.
doi:10.2514/6.2013-1153

[18] Rasuo, B., *Flight Mechanics*, Faculty of Mechanical Engineering, Univ. of Belgrade, Belgrade, Serbia, 2014, pp. 40–89 (in Serbian).

[19] Ringnes, E., and Frost, W., "Analysis of Aerodynamic Coefficients Using Gust Gradient Data: Spanwise Turbulence Effect on Airplane Response," NASA CR 3961, 1986.

[20] Ironside, D., Bramesfeld, G., and Schwochow, J., "Modelling of Wing Drag Reduction due to Structural Dynamics in Atmospheric Gusts," *28th AIAA Applied Aerodynamic Conference*, AIAA Paper 2010-4683, 2010.

[21] Ironside, D., Bramesfeld, G., and Schwochow, J., "Simplified Modelling of Wing Drag Reduction due to Structural Dynamics and Atmospheric Gusts," *26th AIAA Applied Aerodynamic Conference*, AIAA Paper 2008-6238, 2008.

[22] Ulv, M. H., "The Effect of Aeroelasticity Upon Energy Retrieval of a Sailplane Penetrating a Gust," *Technical Soaring*, Vol. 10, No. 4, 1986, pp. 62–72.

[23] Mann, J., "Wind Field Simulation," *Probabilistic Engineering Mechanics*, Vol. 13, No. 4, 1998, pp. 269–282.
doi:10.1016/S0266-8920(97)00036-2

[24] Mann, J., "The Spectral Velocity Tensor in Moderately Complex Terrain," *Journal of Wind Engineering and Industrial Aerodynamics*, Vol. 88, No. 2, 2000, pp. 153–169.
doi:10.1016/S0167-6105(00)00046-5

[25] Kaimal, C., and Finnigan, J., *Atmospheric Boundary Layer Flows, their Structure and Measurement*, Oxford Univ. Press, New York, 1994, pp. 32–63.

[26] Fortuniak, K., and Pawlak, W., "Selected Spectral Characteristics of Turbulence over an Urbanized Area in the Centre of Lodz, Poland," *Boundary-Layer Meteorology*, Vol. 154, No. 1, 2015, pp. 137–156.
doi:10.1007/s10546-014-9966-7

[27] Branlard, E., *Generation of Time Series from a Spectrum: Generation of Wind Time Series from the Kaimal Spectrum, Generation of Wave Time Series from Jonswap Spectrum*, Technical Univ. of Denmark, Lyngby, Denmark, 2010, pp. 1–13.

[28] Database of Wind Characteristics (Online database), Dept. of Wind Energy, Technical Univ. of Denmark, Lyngby, Denmark, 2016, winddata.com [retrieved 15 July 2016].

[29] Kang, H., *Computational Color Technology*, Vol. PM159, SPIE Publications, International Society for Optical Engineering, Bellingham, WA, 2006, pp. 151–159.

[30] Rasuo, B., "Some Analytical and Numerical Solutions for the Safe Turn Manoeuvres of Agricultural Aircraft—An Overview," *Aeronautical Journal*, Vol. 111, No. 1123, 2007, pp. 593–599.
doi:10.1017/S000192400000186X

[31] Stojakovic, P., and Rasuo, B., *Airplane Flight Dynamics Modeling as Demanded by the Control System Design (in Serbian)*, Military Technical Inst., Belgrade, Serbia, 2015, pp. 48–96.

[32] Theodorsen, T., "General Theory of Aerodynamic Instability and Mechanisms of Flutter," NACA Rept. 496, 1935.

[33] Jones, R., "The Unsteady Lift of a Wing of Finite Aspect Ratio," NACA Rept. 681, 1939.

[34] Kholodar, D., and Dowell, H., "The Influence of a Nonzero Angle of Attack and Gust Loads on the Nonlinear Response of a Typical Airfoil Section with a Control Surface Freeplay," *International Journal of Nonlinear Sciences and Numerical Simulation*, Vol. 1, No. 3, 2000, pp. 153–165.
doi:10.1515/IJNSNS.2000.1.3.153

[35] Gili, P., Visone, M., Lerro, A., De Vivo, F., and Scognamiglio, G., "A New Approach for the Estimation of Longitudinal Damping Derivatives: CFD Validation on NACA 0012," *WSEAS Transactions on Fluid Mechanics*, Vol. 10, 2015, pp. 137–145.

[36] Brunton, S., and Rowley, C., "Empirical State-Space Representation for Theodorsen's Lift Model," *Journal of Fluids and Structures*, Vol. 38, 2013, pp. 174–186.
doi:10.1016/j.jfluidstructs.2012.10.005

[37] Saranyasoontorn, K., Manuel, L., and Veers, P., "A Comparison of Standard Coherence Models for Inflow Turbulence with Estimates from Field Measurements," *Journal of Solar Energy Engineering*, Vol. 126, NO. 4, 2004, pp. 1069–1082.
doi:10.1115/1.1797978

[38] IEC/TC88 61400-1, "Wind Turbine Generator Systems Part 1: Safety Requirements," 2nd ed., International Electrotechnical Commission (IEC), Geneva, Switzerland, 1998.